Pre-equilibrium emission of light composite particles in the framework of the exciton model

K. Sato
Division of Physics, Tohoku College of Pharmacy, Komatsushima, Sendai 983, Japan

A. Iwamoto and K. Harada
Japan Atomic Energy Research Institute, Tokai-mura, Naka-gun, Ibaraki 319-11, Japan
(Received 17 May 1983)

The exciton model for the pre-equilibrium emission of light composite particles proposed and applied to the (p,α) reaction of Iwamoto-Harada is further investigated for the energy spectra of the (p,d), (p,t), and (p,^{3}He) reactions with incident energy of several tens of MeV's. Calculated results could reproduce an overall feature of those spectra. The dominance of the pickup-type contribution which occurs in the course of the equilibration process was found to be common for all composite particles. The degree of fitting to the data is excellent for (p,t) reactions to the same extent as for (p,α) reactions, and is somewhat less for the high energy part of energy spectra of (p,^{3}He) and (p,d) reactions. The relative ratio of yields of high energy composite particles was also reproduced fairly well with our model. These facts suggest that the simple reaction mechanism assumed in our model accounts for characteristics of the pre-equilibrium emission of light composite particles.

[NUCLEAR REACTIONS Exciton model, composite particle emission mechanism; (p,d), (p,t), (p,^{3}He) on ^{27}Al, ^{54}Ge, ^{58}Ni, ^{89}Y, ^{120}Sn, ^{197}Au; calculated energy spectra.]

I. INTRODUCTION

In a recent paper[1] two of us (A.I. and K.H.) proposed a model for the pre-equilibrium emission of light composite particles in the framework of the exciton model. (In the following, Ref. 1 will be referred to as I.) It generalizes the exciton model[2–4] so as to include the effect of the intrinsic structure of the emitted particle. This model has been applied to several (p,α) reactions in I and calculated results have nicely reproduced the experimental energy spectra.[5]

In the present paper we apply the model to the (p,d), (p,t), and (p,^{3}He) reactions and calculate those energy spectra in order to study whether the model works well even for the pre-equilibrium emission of light composite particles consisting of two or three nucleons. The model proposed in I introduced the formation factor $F_{l,m}(\epsilon)$ containing the adjustable parameter ΔR which affects the overall normalization of it, and in turn the absolute value of the cross section. It is, therefore, very interesting to see whether or not the model can also give a good fit to d, t, and ^{3}He emission reactions without adjusting the parameter value used in I. In Sec. II we will calculate the formation factor of the composite particle consisting of two or three nucleons quasiclassically with the Fermi gas model in the same way as in I. Support of the use of the quasiclassical method was given by Tonozuka *et al.*,[6] who calculated the alpha formation factor $F_{l,m}(\epsilon)$ quantum mechanically with the shell model and got essentially the same results as I. Calculated results of energy spectra are presented in Sec. III for (p,d), (p,t), and (p,^{3}He) reactions for several targets and incident energies. We will make the comparison between the calculated results and the experimental data. Also, the decompositions of the calculated results to the contributions from various exciton states and to the type of pickup processes are made and discussed. A conclusion is given in Sec. IV.

II. CALCULATION OF COMPOSITE PARTICLE FORMATION FACTOR

In the present section, we will calculate formation factors of the triton, the ^{3}He, and the deuteron following the quasiclassical method with the Fermi gas model described in I. We adopt the method for the following reasons:

(1) We are interested in studying bulk properties of the formation factors.

(2) With this method we can get simple analytic expressions, for the formation factors, which are very convenient for the exciton model analyses of light composite particle emissions.

(3) For the alpha particle the plausibility of the quasiclassical calculation with the rms approximation was shown in Ref. 6. We expect that it also holds for two or three nucleon systems to some extent.

In order to obtain the formation factor of the composite particle consisting of two or three nucleons, we need to calculate the integral

$$F_{l,m}(\epsilon_x)=\frac{1}{(2\pi\hbar)^{3(n_x-1)}}\int_{\substack{|\vec{R}_x|=R_{\rm res}\\ \vec{P}_x:\text{fixed}}}\prod_{i=1}^{n_x-1}d\xi_i d\vec{p}_{\xi_i} \qquad (2.1)$$

which corresponds to Eq. (3.17) in I. In Eq. (2.1) n_x is the number of constituent nucleons to form the composite particle and the range of integration S extends over the phase space volume for the intrinsic motion bounded by the ground state trajectory under the following conditions:

(1) $|\vec{p}_i| \geq p_F$ for $i=1\sim l$

and

$$|\vec{p}_j| < p_F \text{ for } j=l+1\sim n_x \ , \tag{2.2}$$

where p_F is the Fermi momentum;

$$(2)\quad |\vec{r}_i| \leq R_0 \text{ for } i=1\sim n_x \ , \tag{2.3}$$

where $R_0=R_{\rm res}+\Delta R$ is the effective radius of the parent nucleus.

The center of mass coordinate $\vec{R}_x$ of the composite particle x is set equal to the radius $R_{\rm res}$ of the residual nucleus and the center of mass momentum $\vec{P}_x$ is fixed, which is connected to the emission energy of the light composite particle. The explicit definition of the internal coordinate system $(\vec{\xi}_i, \vec{p}_{\xi_i})$ will be given in the following subsections.

A. Triton

First, we will define the coordinate system of the triton as

$$\begin{aligned} &\vec{\xi}_1=\vec{r}_1-\vec{r}_2 \ , \quad \vec{p}_{\xi_1}=\tfrac{1}{2}(\vec{p}_1-\vec{p}_2) \ , \\ &\vec{\xi}_2=\tfrac{1}{2}(\vec{r}_1+\vec{r}_2)-\vec{r}_3 \ , \quad \vec{p}_{\xi_2}=\tfrac{1}{3}(\vec{p}_1+\vec{p}_2-2\vec{p}_3) \ , \end{aligned} \tag{2.4}$$

where $\vec{r}_i$ and $\vec{p}_i$ are the coordinate and the momentum of the ith nucleon. The intrinsic Hamiltonian of the triton is written as

$$h_{\rm t}=\frac{1}{m}p_{\xi_1}^2+\tfrac{1}{4}m\omega^2\xi_1^2+\frac{3}{4m}p_{\xi_2}^2+\tfrac{1}{3}m\omega^2\xi_2^2 \ , \tag{2.5}$$

where m is the nucleon mass and ω the harmonic oscillator parameter. The intrinsic wave function of the triton corresponding to the ground state of this Hamiltonian is given explicitly by

$$\varphi_{\rm t}=\left[\frac{\beta_1}{\pi}\right]^{3/4}\left[\frac{\beta_2}{\pi}\right]^{3/4}\exp\left[-\frac{\beta_1}{2}\xi_1^2-\frac{\beta_2}{2}\xi_2^2\right] \ , \tag{2.6}$$

where

$$\beta_1=\frac{m\omega}{2\hbar} \text{ and } \beta_2=\frac{2}{3}\frac{m\omega}{\hbar} \ . \tag{2.7}$$

The oscillator parameter ω is fixed so as to reproduce the experimental rms charge radius $r_{\rm t}$ of the triton. If we denote by $\vec{R}_{\rm t}$ the center of mass coordinate of the triton, $r_{\rm t}$ is calculated by

$$r_{\rm t}^2=\tfrac{1}{3}\int\sum(\vec{r}_i-\vec{R}_{\rm t})^2|\varphi_{\rm t}|^2 d\vec{\xi}_1 d\vec{\xi}_2=\frac{\hbar}{m\omega} \ . \tag{2.8}$$

The center of mass coordinate $\vec{R}_{\rm t}$ of the triton and the corresponding momentum $\vec{P}_{\rm t}$ are given by

$$\vec{R}_{\rm t}=\tfrac{1}{3}(\vec{r}_1+\vec{r}_2+\vec{r}_3) \ , \tag{2.9}$$

$$\vec{P}_{\rm t}=\vec{p}_1+\vec{p}_2+\vec{p}_3 \ . \tag{2.10}$$

The energy of the triton, $E_{\rm t}$, is given with this $P_{\rm t}$ by the relation

$$E_{\rm t}=\frac{p_{\rm t}^2}{2M_{\rm t}} \ , \tag{2.11}$$

where $M_{\rm t}$ is the mass of the triton. The energy $E_{\rm t}$ is related to the physically observable energy $\epsilon_{\rm t}$ as will be shown later in Eq. (2.25). The ground state trajectory is written as

$$\frac{1}{m}p_{\xi_1}^2+\tfrac{1}{4}m\omega^2\xi_1^2=\tfrac{3}{2}\hbar\omega \tag{2.12}$$

and

$$\frac{3}{4m}\frac{p_{\xi_2}^2}{2}+\tfrac{1}{3}m\omega^2\xi_2^2=\tfrac{3}{2}\hbar\omega \ . \tag{2.13}$$

To calculate the triton formation factor quasiclassically, we must integrate Eq. (2.1) within the phase space bounded by Eqs. (2.12) and (2.13) with particle x taken to be the triton. Before integration, we introduce a new coordinate system for convenience:

$$\begin{aligned} &\vec{\zeta}_1=\tfrac{1}{2}\vec{\xi}_1 \ , \quad \vec{p}_{\zeta_1}=\vec{p}_{\xi_1} \ , \\ &\vec{\zeta}_2=\tfrac{1}{3}\vec{\xi}_2 \ , \quad \vec{p}_{\zeta_2}=\tfrac{1}{2}\vec{p}_{\xi_2} \ . \end{aligned} \tag{2.14}$$

The formation factor is written in the new coordinate system as

$$F_{l,m}(\epsilon_{\rm t})=J\frac{1}{(2\pi\hbar)^6}\int_{\substack{|\vec{R}_{\rm t}|=R_{\rm res}\\ \vec{P}_{\rm t}:\text{fixed}}} d\vec{\zeta}_1 d\vec{p}_{\zeta_1} d\vec{\zeta}_2 d\vec{p}_{\zeta_2} \ , \tag{2.15}$$

where the range of integration s is the region defined in the new coordinate system which corresponds to S in the old one. The Jacobian J of this coordinate transformation is equal to $2^6\cdot 3^3$. In order to perform this twelvefold integration, we will make the approximation of replacing the magnitudes of relative vectors $(\vec{\xi}_i, \vec{p}_{\xi_i})$ with their rms values, the rms approximation, in the same way as I. Then integrals of the space and the momentum coordinates are decoupled. So we rewrite Eq. (2.15) in the product form of them as

$$F_{l,m}(\epsilon_{\rm t})=J\frac{1}{(2\pi\hbar)^6}\left[\frac{5}{3}\right]^6 F^R F_{l,m}^P(\epsilon_{\rm t}) \ , \tag{2.16}$$

where F^R means the coordinate space integral and $F_{l,m}^P(\epsilon_{\rm t})$ the momentum space one. The validity of this approximation will be discussed later. Then we can get the final form of the formation factor which is expressed by elementary functions. We will show, however, only the numerical result of it in the next section for economy of space.

B. ^{3}He

The form of the formation factor for the ^{3}He is quite the same as in the triton case. But the rms radius $r_{^3\mathrm{He}}$ is set equal to 1.88 fm instead of the 1.7 fm of the triton,[8] which corresponds to the change of the oscillator parameter, as is shown in Table I.

C. Deuteron

The coordinate system, the intrinsic Hamiltonian, and the intrinsic wave function of the deuteron are defined by

$$\vec{\xi}=\vec{r}_1-\vec{r}_2\ ,\quad \vec{p}_\xi=\tfrac{1}{2}(\vec{p}_1-\vec{p}_2)\ , \tag{2.17}$$

$$h_t=\frac{1}{m}p_\xi^2+\tfrac{1}{4}m\omega^2\xi^2\ , \tag{2.18}$$

and

$$\varphi_d=\left[\frac{\beta}{\pi}\right]^{3/4}\exp\left[-\frac{\beta}{2}\xi^2\right]\ , \tag{2.19}$$

respectively. The center of mass coordinate of the deuteron $\vec{R}_d$ and the corresponding momentum $\vec{P}_d$ are given by

$$\vec{R}_d=\tfrac{1}{2}(\vec{r}_1+\vec{r}_2)\ ,\quad \vec{P}_d=\vec{p}_1+\vec{p}_2\ . \tag{2.20}$$

We will fix the oscillator parameter ω from the rms radius r_d of the deuteron which is taken from Ref. 7. The relation between the rms radius r_d and the oscillator parameter ω of the deuteron is given by

$$r_d=\tfrac{1}{2}\int\sum(\vec{r}_i-\vec{R}_d)^2\,|\,\varphi_d\,|^2 d\,\vec{\xi}=\frac{3}{4}\frac{\hbar}{m\omega}\ . \tag{2.21}$$

The ground state trajectory is written as

$$\frac{1}{m}p_\xi^2+\tfrac{1}{4}m\omega^2\xi^2=\tfrac{3}{2}\hbar\omega\ . \tag{2.22}$$

To calculate the deuteron formation factor quasiclassically, the following coordinate transformation is performed:

$$\vec{\zeta}=\tfrac{1}{2}\vec{\xi}\ ,\quad \vec{p}_\zeta=\vec{p}_\xi\ , \tag{2.23}$$

and the formation factor is now written as

$$F_{l,m}(\epsilon_d)=J\frac{1}{(2\pi\hbar)^3}\int_{\substack{|\vec{R}_d|=R_{\mathrm{res}}\\ \vec{P}_d:\mathrm{fixed}}} d\,\vec{\zeta}\,d\,\vec{p}_\zeta\ . \tag{2.24}$$

The Jacobian J is equal to 2^3. If we adopt the rms approximation, double integrals of the space and the momentum coordinates are decoupled as noted in Sec. II A, and we can easily obtain a very simple expression for the formation factor $F_{l,m}(\epsilon_d)$. For the two nucleon system such as the deuteron, however, we can integrate the right-hand side of Eq. (2.24) analytically without making the rms approximation. The result will be presented in the Appendix. It is expected that the error due to the rms approximation becomes largest in the deuteron system, since this type of approximation is thought to become worse the smaller the number of degrees of freedom. The comparison of the two kinds of the integration in the deuteron system is, therefore, worthy to check the validity of the approximation.

D. Properties of the formation factor

We show in Figs. 1–3 the formation factors $F_{l,m}$ of the triton, the ^{3}He, and the deuteron, respectively, as a function of the particle energy. Two energy scales on the abscissa stand for the energy E_x in the Fermi gas given by, for example, Eq. (2.11) for the triton, and the energy ϵ_x which is physically observable. They are related to each other by the relation

$$\epsilon_x=E_x-n_x\mathscr{E}_F+E_x^{\mathrm{int}}+Q_x\ , \tag{2.25}$$

with

$$E_x^{\mathrm{int}}=\tfrac{1}{2}\tfrac{3}{2}(n_x-1)\hbar\omega\ ,$$

where $\mathscr{E}_F$ is the nucleon Fermi energy and E_x^{int} the intrinsic kinetic energy of the composite particle x, and Q_x the binding energy. In Figs. 1–3, however, we plot the case for $Q_x=0$. Thus in the realistic case, the abscissa shifts to the right or left by an amount $|\,Q_x\,|$. We use the value $\mathscr{E}_F=33.5$ MeV throughout our calculation. Table I shows the rms radii r_x,[7,8] the harmonic oscillator parameters $\hbar\omega$, and the experimental separation energies Q_x of the composite particles from six different targets used in our calculation. Those values of the alpha particle taken from I are also added for reference purposes. The absolute value of $F_{l,m}$ depends sensitively on the parameter $\Delta R=R_0-R_{\mathrm{res}}$ through the surface condition Eq. (2.3). Once we make the rms approximation, the functional form of $F_{l,m}$ as a function of ϵ_x becomes independent of ΔR and only the overall normalization factor depends on ΔR, as is seen from Eq. (2.16). For the value of $\Delta R\gg r_x$, the condition Eq. (2.3) is no longer effective, and this leads to

$$\sum_{l+m=n_x}F_{l,m}(\epsilon_x)=1\ , \tag{2.26}$$

which corresponds to Eq. (3.30) in I. Figures 1 and 2 show the numerical results for this case. The formation

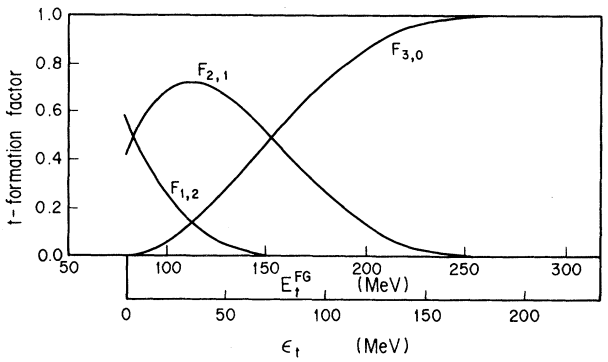

FIG. 1. The triton formation factor $F_{l,m}$ for $\Delta R\gg r_t$ as a function of the triton energy ϵ_t. In the abscissa the triton energy E_t in the Fermi gas is also shown. The relation between ϵ_t and E_t is given in the text, although we set $Q_t=0$ in the figure. $F_{l,m}$'s are normalized to unity in a classical manner.

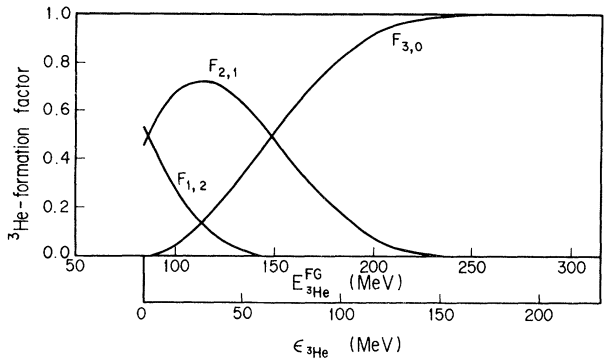

FIG. 2. Same as Fig. 1, but for ^{3}He.

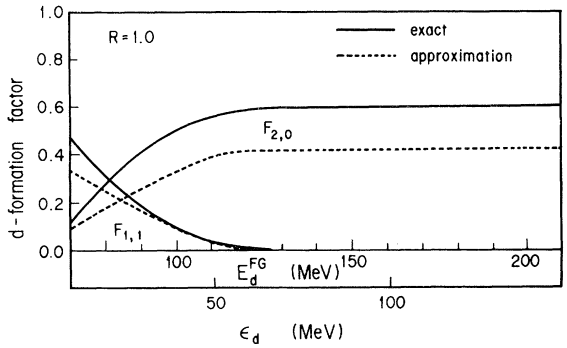

FIG. 3. The deuteron formation factor $F_{l,m}$ for $\Delta R = 1.0$ fm as a function of the deuteron energy ϵ_d. The solid curves correspond to the calculation with the exact integration and the dashed curves to the calculation with the rms approximation.

factors $F_{l,m}$ used in our calculation for energy spectra are calculated fixing the parameter ΔR to 1.0 fm, and the sum of their values are listed in Table II.

In the deuteron formation factor shown in Fig. 3, the solid curve is the one for the exact integration and the dashed curve is for the rms approximation. The solid curve changes with ΔR not only in the absolute value but also in the shape since the momentum and the coordinate variables are coupled in this case. Therefore, we show two results calculated with $\Delta R = 1.0$ fm.

In the next section, we deal with the energy spectra of the triton, the ^{3}He, and the deuteron emitted with several tens of MeV's of energy. For the triton and the ^{3}He in this energy region, the values of $F_{3,0}$ are about equal to or less than $\frac{1}{5}$ of total $\sum F_{l,m}$, and $F_{2,1}$ are much larger than $F_{3,0}$, as can be seen from Figs. 1 and 2. For the deuteron, the value of $F_{2,0}$ is over half the total of $\sum F_{l,m}$ there and the component $F_{1,1}$ comes to have a significant value in the energy region below about 40 MeV. The components $F_{0,3}$ and $F_{0,2}$ are not shown in these figures because they have the finite values only for $\epsilon_x < 0$ region. The value of ϵ_x at which $F_{n_x,0}$ takes the asymptotic value is strongly dependent on the value of $\hbar\omega$, the oscillator parameter of the composite particle, as well as on the number of intrinsic degrees of freedom. For the deuteron, which is the quite loosely bound system and is assigned a small $\hbar\omega$ value, the $F_{2,0}$ component is dominant in this energy region. For the triton and the ^{3}He, on the other hand, pickup-type components ($F_{2,1}$,$F_{1,2}$) are very large, although smaller than in the case of the alpha particle. Comparing Fig. 1 with Fig. 2, we can see a small but non-negligible difference between them, which reflects the fact that the ^{3}He is a little more loosely bound system than the triton. This difference is partly responsible for the difference between their relative yield, as we shall see in the next section.

Finally we comment on the difference between the exact and the rms approximate calculations in the formation factor of the deuteron. As is clearly seen from Fig. 3, the rms approximation formation factor is less in the absolute value and in the gradient than the exact one. This tendency is enhanced as $\Delta R \to 0$. Fortunately this discrepancy does not greatly affect the cross section, as will be shown in the next section.

III. NUMERICAL CALCULATION OF ENERGY SPECTRA AND COMPARISON WITH EXPERIMENTAL DATA

In this section, we show the calculated results of the angle integrated cross sections for the pre-equilibrium emissions of the triton, the ^{3}He, and the deuteron. Owing to the use of the "never come back approximation," our calculation of energy spectra does not contain the equilibrium and near-equilibrium components. In the following calculation, we always start from the 2p-1h state and sum up the contributions until the one of the 6p-5h state. Actually, the states above the 4p-3h state give negligible contributions to the high energy spectra. As for the parameter values relevant of the exciton model, we use the same

TABLE I. The rms radius r_x and the harmonic oscillator parameter $\hbar\omega$ of light composite particles x are listed. The separation energy Q_x of the light composite particle x from the parent nucleus is also listed for ^{27}Al, ^{54}Fe, ^{58}Ni, ^{89}Y, ^{120}Sn, and ^{197}Au targets. The values for the alpha particle are taken from Ref. 1.

Particle	r_x (fm)	$\hbar\omega$ (MeV)	Q_x (MeV) for targets ^{27}Al	^{54}Fe	^{58}Ni	^{89}Y	^{120}Sn	^{197}Au
d	1.96	8.1	−22.4	−16.4	−13.4	−17.6	−12.7	−13.0
t	1.7	14.4	−27.5	−20.6	−17.4	−20.5	−12.9	−13.4
^{3}He	1.88	11.7	−23.2	−18.2	−15.3	−18.8	−17.1	−13.1
α	1.6	18.2	−10.0	−8.2	−4.8	−6.7	−3.1	1.3

TABLE II. The values of $\sum F_{l,m}$ for light composite particles in the six proton plus target systems. The parameter ΔR is fixed to be 1.0 fm.

Particle	Target ^{27}Al	^{54}Fe	^{58}Ni	^{89}Y	^{120}Sn	^{197}Au
d[a]	0.55	0.57	0.57	0.59	0.59	0.60
d[b]	0.35	0.38	0.38	0.40	0.41	0.43
t	0.27	0.31	0.31	0.33	0.34	0.36
^{3}He	0.18	0.22	0.22	0.24	0.25	0.27
α	0.36	0.41	0.41	0.43	0.45	0.47

[a]Calculation with the exact integration.
[b]Calculation with the rms approximation.

values as adopted in I. Those are the single particle level density, spreading width, and absorption cross sections of the nucleon, and the complex particle and radius parameter of the target nucleus, and so on. The quantity ΔR defined in Eq. (2.3) is set to be 1.0 fm throughout the present calculation.

Numerical calculations have been performed for the proton incident reactions on targets of ^{27}Al, ^{54}Fe, ^{58}Ni, ^{89}Y, ^{120}Sn, and ^{197}Au. In Fig. 4, we show the results for the deuteron, the triton, and the ^{3}He spectra from the proton incident reactions on ^{120}Sn with $E_p = 62$ MeV. We see from this figure that the data[5] are well reproduced by our calculation, although we see some discrepancy in the high energy part, especially for the deuteron emission. In this figure, we also show the calculated result with the rms approximation for the deuteron by a dotted curve. It will be discussed later. For reference, the calculated energy spectra of the proton and the alpha particle which are taken from I are also included in Figs. 4–7.

Next, as examples of the heavier and the lighter target

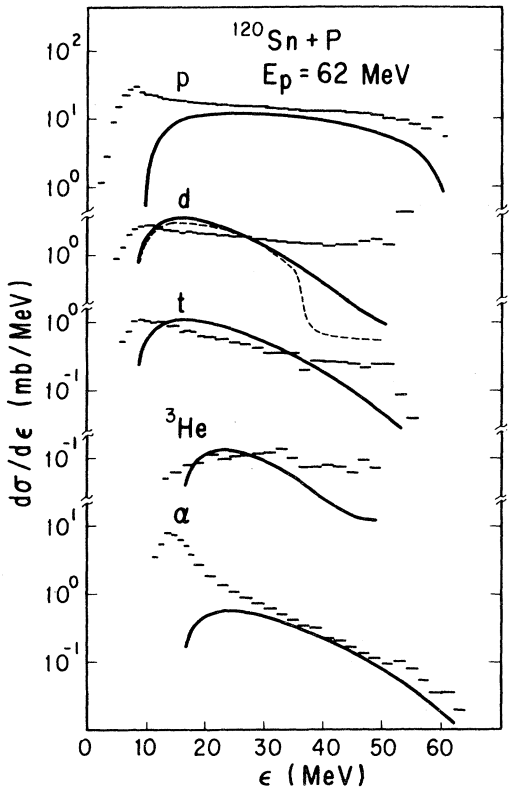

FIG. 4. Angle-integrated energy spectra for (p,d), (p,t), (p, ^{3}He), and (p,α) reactions on ^{120}Sn with $E_p = 62$ MeV. The bar graphs show the data and the solid curves represent our calculated results. In this figure, we also show the calculated result with the rms approximation for the deuteron by a dotted curve. Types of emitted composite particles are indicated near the appropriate curves.

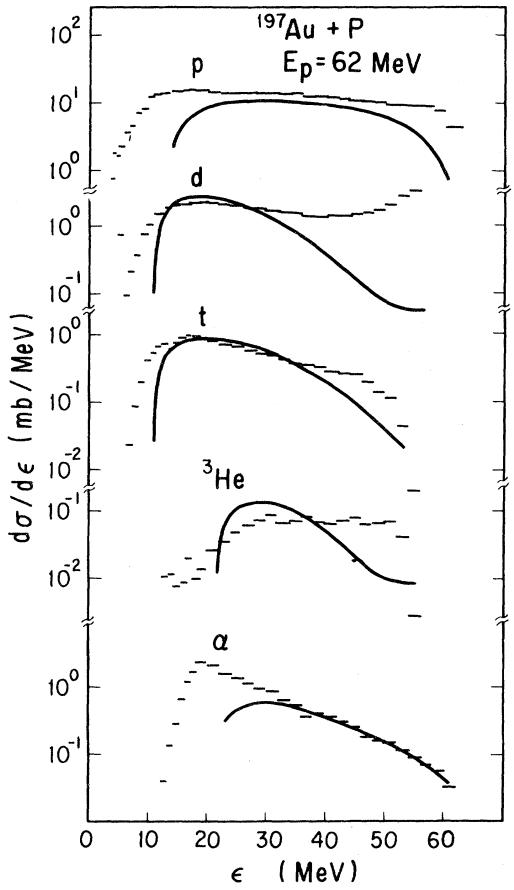

FIG. 5. Same as Fig. 4, but for a ^{197}Au target.

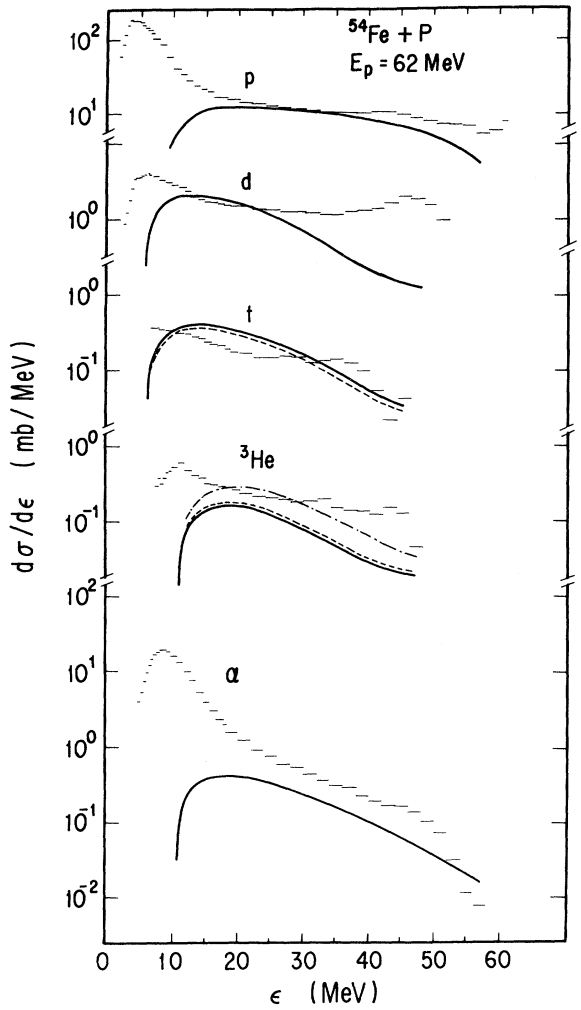

FIG. 6. Same as Fig. 4, but for a ^{54}Fe target. Dashed curves are the calculated results in which the excitation energy U of the residual nucleus is replaced by $U+1.6$ MeV for the ^{3}He emission and by $U-1.6$ MeV for the triton one. The dash-dotted curve for the ^{3}He is the calculation taking the rms radius to be 1.7 fm.

nuclei, calculated results for reactions on ^{197}Au and ^{54}Fe with $E_p=62$ MeV are shown in Figs. 5 and 6, respectively. As is seen from these figures, the quality of the fitting is better for an Au target than for one of Sn. The fitting for the Fe target is nearly the same as for that of Sn. Better fitting for a heavy target gives favorable support to our calculation since the heavier the system, the better the Fermi gas model works. We see in Figs. 4 and 5 that the experimental yields of the ^{3}He are several times less than those of the triton for Sn and Au targets. This fact is well reproduced by our calculations. The lower yield of the ^{3}He originates from the smaller $F_{1,2}$ of ^{3}He by about a factor of 2 than those of the triton and the higher Coulomb barrier.

The experimental energy spectra of the ^{3}He are different in shape from those of the triton and the alpha particle in heavy target nuclei, as is seen from Figs. 4 and 5.

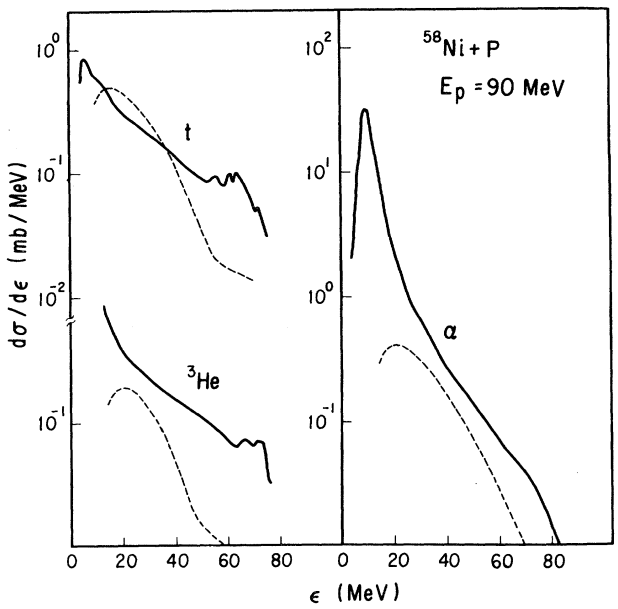

FIG. 7. Angle-integrated energy spectra for (p,t), (p,^{3}He), and (p,α) reactions on ^{58}Ni with $E_p=90$ MeV. The solid curves show the data and the dotted ones represent our calculated results.

This can be understood by noting their differences in Coulomb barriers and binding energies. For the statistical emission of complex particles the lower end (the minimum of the emission energy) strongly depends on the value of the Coulomb barrier, and the upper end (the maximum of the emission energy) on that of the binding energy. The lower ends of the ^{3}He and the alpha particle are about twice as large as that of the triton. On the other hand, the upper end for the emission of the triton and the ^{3}He is about 10 MeV less than that of the alpha particle (see Table I). These make the energy region for the ^{3}He emission narrower than those for the triton and the alpha particle, and lead to less yield of the ^{3}He. Then the direct type reaction seems to have large influence on its energy spectra. In light targets such as ^{54}Fe, on the contrary, the suppression of the statistical emission of the complex particle by the Coulomb barrier is expected to be weak. This brings the similar behavior of the energy spectra, both in absolute value and in shape for the triton and the ^{3}He, as is seen in Fig. 6. Figure 6 shows an underestimation of about 50% in the calculated cross section for the ^{3}He, in contrast to a small overestimation for the triton as compared with the data. The ^{3}He emission leads to the odd-odd residual nucleus, but the triton emission leads to the even-even nucleus. Dashed curves in Fig. 6 are obtained by replacing the excitation energy U of the residual nucleus after the ^{3}He emission by $U+1.6$ MeV and that after the triton emission by $U-1.6$ MeV, in the estimation of the level density of the residual nucleus. For the ^{3}He emission, furthermore, the calculation taking the same rms radius as the one of the triton is performed and is shown in Fig. 6 by the dash-dotted curve. These trials suggest that the discrepancies seen in the cases for the tri-

ton and the ^{3}He emissions can be removed mostly by the adjustment (to a not considerable extent) of parameters. As for calculated results for the reactions on ^{89}Y and ^{27}Al with $E_p=62$ MeV, we have found the same quality of fitting as in the cases of Sn and Fe, respectively, although the agreement of the absolute cross section for the Al target is a little worse than that for the Fe target.

In order to see how the result changes as the incident energy increases, we show in Fig. 7 the result for ^{58}Ni with $E_p=90$ MeV. The solid curves are the experimental data[9] and the dotted ones represent our calculated results. Calculated results can almost reproduce the absolute values of the angle integrated cross sections, except those in the high energy region. From Figs. 6 and 7 it can be seen that the underestimation of the highest energy spectra becomes large with the incident energy. This fault seems to come from the fact that there is no counting in our model of the nonstatistical component which is expected to increase with the incident energy. As an example for a low incident energy, we have calculated the spectra for ^{54}Fe with $E_p=39$ MeV, and find a nice fitting to the data, although this is not shown in the figure.

Together with the results shown so far, we can say that, below incident energy with several tens of MeV's, our exciton model calculation nicely reproduces the experimental data for the pre-equilibrium emission of light composite particles, except the highest energy part of the deuteron spectra and of the ^{3}He. If we note that the parameter ΔR is always fixed to be 1.0 fm in all cases, the agreement between our calculated results and the data is considered to be remarkable. As the incident energy increases ($\simeq$90 MeV), the discrepancy between the data and our calculated results in the highest energy part of the spectra becomes larger for all composite particles. It is conceivable that the nonstatistical reaction mechanism will play an important role in such a high incident energy region.

In order to see the structure of our calculated results, we show in Fig. 8 the decomposition of the result for the triton emission shown in Fig. 4 into the contributions from various particle-hole states. As is clear from this figure, the 2p-1h state is most responsible for the high energy triton spectra. As the energy decreases, the contributions from 3p-2h and 4p-3h become more effective. The similar decomposition of the result for the deuteron emission shown in Fig. 4 is given in Fig. 9. From this figure we see that the behavior of each component is very similar to the one of the triton. Though not shown in the figure, we can say the same thing for the ^{3}He emission. Our result, together with the result for alpha emission in I, indicates that the behavior seen in Figs. 8 and 9 is a common feature of the present model.

In order to see the relative importance of various $F_{l,m}$

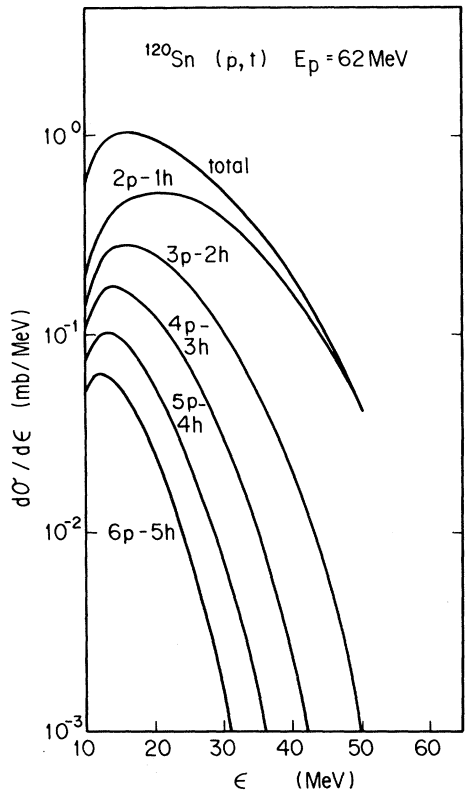

FIG. 8. Decomposition of the calculated energy spectra of the ^{120}Sn(p,t) reaction with $E_p=62$ MeV into the contributions from various particle-hole states. The curves labeled by 2p-1h, 3p-2h, etc., indicate a two-particle one-hole, three-particle two-hole, etc., state of the parent nucleus.

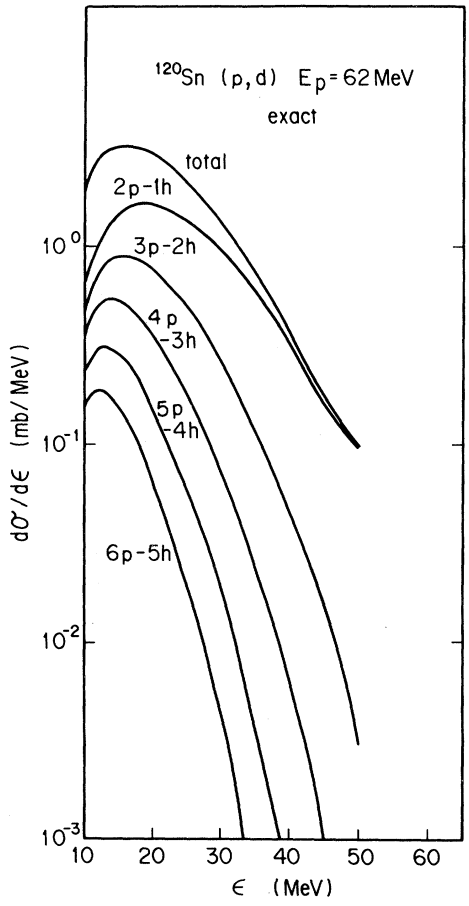

FIG. 9. Same as Fig. 8, but for the deuteron emission.

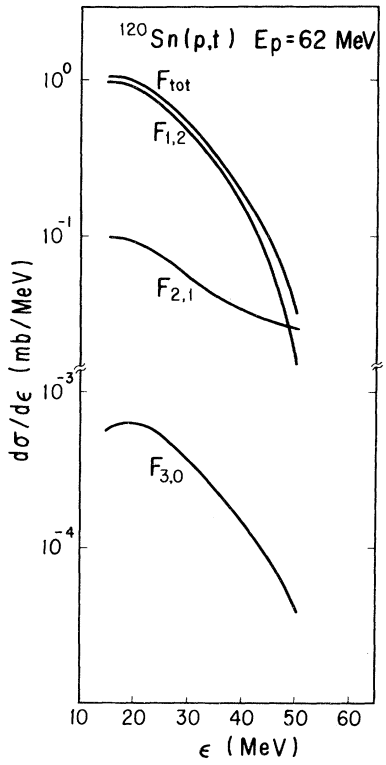

FIG. 10. Decomposition of the calculated energy spectra of the ^{120}Sn(p,t) reaction with $E_p = 62$ MeV to various components of the triton internal structure. The curve labeled $F_{l,m}$ is the contribution to the cross section of the triton formed from l-particles above the Fermi level and m particles below. F_{tot} means the total sum.

components, we give in Fig. 10 the decomposition of the triton energy spectra shown in Fig. 4 into various $F_{l,m}$ ones. We see that the dominant contribution comes from the $F_{1,2}$ component, which corresponds to a two-particle pickup-type reaction. The contribution of the $F_{2,1}$ component, which corresponds to a one-particle pickup type, is several times less than that of $F_{1,2}$, except the highest energy region. These can be easily understood by comparing the level densities of the residual nuclei in both cases. Our calculation indicates that the contribution of the triton formed by three particles above the Fermi level is very small. The same situation holds for the ^{3}He, although it is not shown in a figure. Kalbach[10] has pointed out the importance of the pickup reactions in calculating spectral shapes, based on a purely semiempirical approach. Our Fig. 10 gives a physical interpretation and supports her argument. In Fig. 11, we show the same decomposition for the deuteron emission presented in Fig. 4. In this figure, the dominance of the pickup type $F_{1,1}$ component is also clearly seen. In the energy region below about 35 MeV, two calculations for $F_{1,1}$ with and without the rms approximation give nearly the same results. In the region above 35 MeV, on the contrary, a large discrepancy of about a factor of 3 occurs. This stems from the more

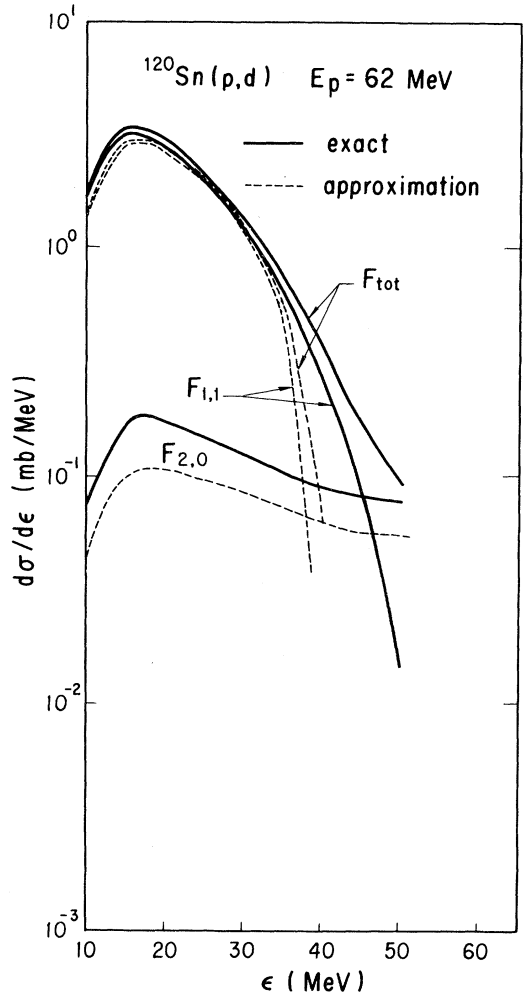

FIG. 11. Same as Fig. 10, but for the deuteron emission. The solid curves correspond to the result with the exact integration and the dashed ones that with the rms approximation.

rapid falling off of $F_{1,1}$ obtained with the rms approximation than that with the exact integration. We expect, however, that such a discrepancy in the high energy region becomes less for three- and four-nucleon systems because their internal degrees of freedom are larger and the rms approximation works better. The underestimation of the high energy spectra seen in every system (Figs. 4—7) is especially large for the deuteron. It is conceivable that the direct neutron pickup reaction which is not counted in our model will give a large contribution in the high energy region.[11] The remaining shortage seems to be ascribed to our quasiclassical estimation for the formation factor. This method neglects quantal fluctuation and penetration, and is considered to be the worst for the system of the smallest $\hbar\omega$ and of the fewest internal degrees of freedom (see Table I).

IV. CONCLUSION

In the present work, the exciton model for the preequilibrium emission of light composite particles proposed

in I was applied to the (p,d), (p,t), and (p,^{3}He) reactions with an incident energy of several tens of MeV's. As was shown, calculated results could nicely reproduce the overall features of those energy spectra. The relative ratio of yields of high energy composite particles is also reproduced fairly well. The fitting to the data was within a factor of 2 or 3 for almost all systems without adjusting the parameter values used in I. It is concluded that our model can account for characteristics of the emitted pre-equilibrium d, t, and ^{3}He spectra as well as the α particle and can point out the importance of the pickup-type mechanism during equilibration. The energy spectra in the highest energy region are, however, underestimated by our model, especially for the deuteron.

ACKNOWLEDGMENTS

We are indebted to Prof. S. Yoshida, Prof. M. Ichimura, Prof. T. Kishimoto, and Dr. T. Nomura for valuable discussions and comments. One of us (K.S.) thanks the members of the Nuclear Theory Group at Tohoku University for useful comments.

APPENDIX

In this appendix we present the expression for the exactly integrated deuteron formation factor $F_{l,m}(\epsilon_d)$. The convention of $\hbar=1$ is used. For the present purpose we consider the integral

$$I=\int' d\vec{p}_\xi \int' d\vec{\xi}\,'$$

in the region surrounded by the ground state trajectory (2.22) under the conditions (2.2) and (2.3). Let us define the radius of the target nucleus $R^0=R_{\rm res}$, the momentum $P=P_d/2$, the intrinsic energy $E=(3/2)\omega$, and the upper end point in the $\vec{\xi}$ integral as

$$\xi_0(p_\xi)\equiv\left[\frac{1}{m\omega^2}\left[E-\frac{1}{m}p_\xi^2\right]\right]^{1/2}\le\xi_0^{\max}\equiv\left[\frac{E}{m\omega^2}\right]^{1/2}. \tag{A1}$$

First we consider the $\vec{\xi}$ integral. If we define the angle α between two vectors $\vec{R}$ and $\vec{\xi}$, the conditions (2.3) for $\vec{r}_1$ and $\vec{r}_2$ are written as

$$r_1^2=R^2+\xi^2-2R\xi\cos\alpha<R_0^2$$

or

$$\cos\alpha=\frac{R^2+\xi^2-r_1^2}{2R\xi}>\xi_L\equiv\frac{R^2+\xi^2-R_0^2}{2R\xi} \tag{A2}$$

and

$$r_2^2=R^2+\xi^2+2R\xi\cos\alpha<R_0^2$$

or

$$\cos\alpha<\xi_U\equiv\frac{R_0^2-R^2-\xi^2}{2R\xi}. \tag{A3}$$

Then we have

$$\int' d\vec{\xi}=\int_0^{\xi_0(p_\xi)}\xi^2 d\xi\int' d\Omega_\xi=\int_0^{\xi_0(p_\xi)}\xi^2 d\xi\,2\pi\int_{\xi_L}^{\xi_U}d\cos\alpha\,. \tag{A4}$$

Now noticing

$$\xi_U-1=\frac{(R_0-R-\xi)(R_0+R+\xi)}{2R\xi}, \tag{A5}$$

we have

$$\begin{aligned}&\xi_U<1\ \text{ for }\Delta R=R_0-R<\xi\,,\\&\xi_U>1\ \text{ for }\Delta R=R_0-R>\xi\,.\end{aligned} \tag{A6}$$

Using the above equations, we can divide the $\vec{\xi}$ integral Eq. (A4) into the following three cases:

(i) $\Delta R>\xi_0^{\max}$:

$$\int' d\vec{\xi}=\frac{4\pi}{3}\xi_0^3\,;$$

(ii) $\xi_0^{\max}\ge\xi_0(p_\xi)>\Delta R$:

$$\begin{aligned}\int' d\vec{\xi}&=\int_0^{\Delta R}\xi^2 d\xi\,4\pi+\int_{\Delta R}^{\xi_0(p_\xi)}\xi^2 d\xi\,4\pi r_U\\&=C_0+C_2r_0^2+C_4r_0^4\,;\end{aligned} \tag{A7}$$

(iii) $\xi_0^{\max}\ge\Delta R>\xi_0(p_\xi)$:

$$\int' d\vec{\xi}=\frac{4\pi}{3}\xi_0^3\,;$$

where

$$\begin{aligned}C_0&=\frac{4\pi}{3}\Delta R^3+\frac{\pi}{R_0}\,,\\C_2&=\pi\Delta R\left[2+\frac{\Delta R}{R_0}\right],\\C_4&=-\frac{\pi}{2R_0}\,.\end{aligned} \tag{A8}$$

Next we consider the $\vec{p}_\xi$ integral. Let us define the angle β between two vectors $\vec{p}$ and $\vec{p}_\xi$. Then in the calculation of $F_{2,0}$ the conditions (2.2) for $\vec{p}_1$ and $\vec{p}_2$ become

$$p_1^2=p^2+p_\xi^2-2pp_\xi\cos\beta>p_F^2$$

or

$$\cos\beta=\frac{p^2+p_\xi^2-p_1^2}{2pp_\xi}<p_U\equiv\frac{p^2+p_\xi^2-p_F^2}{2pp_\xi} \tag{A9}$$

and

$$p_2^2=p^2+p_\xi^2+2pp_\xi\cos\beta>p_F^2$$

or

$$\cos\beta>p_L\equiv\frac{p_F^2-p^2-p_\xi^2}{2pp_\xi}\,. \tag{A10}$$

Noticing

$$p_U - 1 = \frac{(p - p_\xi - p_F)(p - p_\xi + p_F)}{2pp_\xi} , \tag{A11}$$

we have

$$\begin{aligned} &p_U < 1 \quad \text{for } p - p_F < p_\xi , \\ &p_U > 1 \quad \text{for } p - p_F > p_\xi . \end{aligned} \tag{A12}$$

Introducing the momentum p_0 as

$$\begin{aligned} &p_0 = 0 \quad \text{for } \Delta R > \zeta_0^{\max} , \\ &p_0 = \sqrt{m(E - m\omega^2 \Delta R^2)} \quad \text{for } 0 < \Delta R \le \zeta_0^{\max} , \end{aligned} \tag{A13}$$

we have the following correspondences:

$$\begin{aligned} &\Delta R < \zeta_0(p_\xi) \leftrightarrow p_\xi < p_0 , \\ &\Delta R > \zeta_0(p_\xi) \leftrightarrow p_\xi > p_0 . \end{aligned} \tag{A14}$$

Then the integration is performed separately according to the following four cases:

(i) $p_F + \sqrt{mE} < P$:

$$\begin{aligned} I &= 4\pi \int_0^{\sqrt{mE}} p_\xi^2 dp_\xi \int' d\vec{r} \\ &= 4\pi \int_0^{p_0} p_\xi^2 dp_\xi (C_0 + C_2\xi_0^2 + C_4\xi_0^4) + 4\pi \int_{p_0}^{\sqrt{mE}} p_\xi^2 dp_\xi \frac{4\pi}{3}\xi_0^3 ; \end{aligned}$$

(ii) $p_F + p_0 \le P < P_F + \sqrt{mE}$:

$$I = 4\pi \int_0^{p_0} p_\xi^2 dp_\xi (C_0 + C_2\xi^2 + C_4\xi^4) + 4\pi \int_{p_0}^{p - p_F} p_\xi^2 dp_\xi \frac{4\pi}{3}\xi_0^3 + 2\pi \int_{p - p_F}^{\sqrt{mE}} p_\xi^2 dp_\xi \frac{p^2 + p_\xi^2 - p_F^2}{pp_\xi} \frac{4\pi}{3} ; \tag{A15}$$

(iii) $p_F \le P \le P_F + p_0$:

$$\begin{aligned} I = {} & 4\pi \int_0^{p - p_F} p_\xi^2 dp_\xi (C_0 + C_2\xi_0^2 + C_4\xi_0^4) + 2\pi \int_{p - p_F}^{p_0} p_\xi^2 dp_\xi \frac{p^2 + p_\xi^2 - p_F^2}{pp_\xi} (C_0 + C_2\xi_0^2 + \xi_0^4) \\ & + 2\pi \int_{p_0}^{\sqrt{mE}} p_\xi^2 dp_\xi \frac{p^2 + p_\xi^2 - p_F^2}{pp_\xi} \frac{4\pi}{3}\xi_0^3 ; \end{aligned}$$

(iv) $P < p_F$:

$$\begin{aligned} I = {} & \int_0^{p_0} p_\xi^2 dp_\xi 2\pi \frac{p^2 + p_\xi^2 - p_F^2}{pp_\xi} (C_0 + C_2\xi_0^2 + C_4\xi_0^4) \\ & + \int_{p_0}^{\sqrt{mE}} p_\xi^2 dp_\xi 2\pi \frac{p^2 + p_\xi^2 - p_F^2}{pp_\xi} \frac{4\pi}{3}\xi_0^3 . \end{aligned}$$

Similarly the $\vec{p}_\xi$ integral in the calculation of $F_{1,1}$ can be performed separately according to the four cases. Carrying out those $\vec{p}_\xi$ integrations and rearranging the overall normalization we finally get expressions for $F_{l,m}$. In order to write the formation factor $F_{l,m}$ in a compact form, we introduce the following four functions:

$$Q_1(x) = \frac{16}{81\pi} \frac{1}{(m\omega)^3} \left[-8x(mE - x^2)^{5/2} + 2mEx(mE - x^2)^{3/2} + 3(mE)^2 x(mE - x^2)^{1/2} + 3(mE)\sin^{-1}\frac{x}{\sqrt{mE}} \right] , \tag{A16}$$

$$Q_2(x) = \frac{128}{27\pi} \frac{1}{(m\omega)^3 p} \left[\tfrac{1}{5}(p^2 - p_F^2 + mE)(mE - x^2)^{5/2} - \tfrac{1}{7}(mE - x^2)^{7/2} \right] , \tag{A17}$$

$$Q_3(x) = \frac{64}{4\pi^2} x^3 \left\{ \tfrac{1}{3}C_0 + C_2 \frac{1}{(m\omega)^2} (\tfrac{1}{3}mE - \tfrac{1}{5}x^2) + C_4 \frac{1}{(m\omega)^4} \frac{1}{7} \left[(x^2 - mE)^2 - \tfrac{4}{5}mE(x^2 - mE) + \tfrac{8}{15}(mE)^2 \right] \right\} , \tag{A18}$$

$$\begin{aligned} Q_4(x) = {} & \frac{16}{9\pi^2 p} \left\{ C_0 x^2 (p^2 - p_F^2 + \tfrac{1}{2}x^2) + \frac{C_2 x^2}{(m\omega)^2} \left[(p^2 - p_F^2)(mE - \tfrac{1}{2}x^2) + x^2 \left[\tfrac{1}{2}mE - \frac{x^2}{3} \right] \right] \right. \\ & \left. + \frac{C_4}{3(m\omega)^4} (x^2 - mE)^3 (p^2 - p_F^2 + x^2 + \tfrac{1}{3}mE) \right\} . \end{aligned} \tag{A19}$$

Both $F_{2,0}$ and $F_{1,1}$ are classified into four groups according to the value of the momentum P as follows:

$F_{2,0}$ (two particles are above the Fermi level):

(i) $p_F+\sqrt{mE}<P$:

$$F_{2,0}=1-Q_1(p_0)+Q_3(p_0);$$

(ii) $p_F+p_0\le P<p_F+\sqrt{mE}$:

$$F_{2,0}=Q_1(p-p_F)-Q_1(p_0)+Q_2(p-p_F)+Q_3(p_0); \tag{A20}$$

(iii) $p_F\le P<p_F+p_0$:

$$F_{2,0}=Q_2(p_0)+Q_3(p-p_F)+Q_4(p_0)-Q_4(p-p_F);$$

(iv) $P<p_F$:

$$F_{2,0}=Q_4(p_0)-Q_4(0)+Q_2(p_0)\ .$$

$F_{1,1}$ (one particle is above the Fermi level and the remaining one is below):

(i) $p_F+\sqrt{mE}<P$:

$$F_{1,1}=0;$$

(ii) $p_F+p_0\le P<p_F+\sqrt{mE}$:

$$F_{1,1,}=1-Q_1(p-p_F)-Q_2(p-p_F); \tag{A21}$$

(iii) $p_F\le P<p_F+p_0$:

$$F_{1,1,}=1-Q_1(p_0)-Q_2(p_0)+Q_4(p-p_F)-Q_4(p_0)+Q_3(p_0)-Q_3(p-p_F);$$

(iv) $P<p_F$:

$$F_{1,1}=1-Q_2(p_0)-Q_1(p_0)+Q_3(p_0)+Q_4(0)-Q_4(p_0)\ .$$

[1]A. Iwamoto and K. Harada, Phys. Rev. C 26, 1821 (1982).
[2]J. J. Griffin, Phys. Rev. Lett. 17, 478 (1966).
[3]C. K. Klein, Nucl. Phys. A193, 417 (1972); A210, 590 (1973).
[4]M. Blann, Annu. Rev. Nucl. Sci. 25, 123 (1975).
[5]F. E. Bertrand and R. W. Peelle, Phys. Rev. C 8, 1045 (1973).
[6]I. Tonozuka, A. Iwamoto, and K. Harada, Japan Atomic Energy Research Institute Report JAERI-M 83-057 (1983).
[7]R. Hofstadter, *Nuclear and Nucleon Structure* (Benjamin, New York, 1963), p. 220.
[8]H. Callard *et al.*, Phys. Rev. 138, B57 (1965).
[9]J. R. Wu and C. C. Chang, Phys. Rev. C 17, 1540 (1978).
[10]C. Kalbach, Z. Phys. A 283, 401 (1977).
[11]O. Dragun *et al.*, Phys. Lett. 119B, 25 (1982).